Fachtagung "Experimentelle Strömungsmechanik"
5.–7. September 2023, München

Messung der Winkelgeschwindigkeit von schlanken, gekrümmten Fasern der Kolmogorov Größe

Angular velocity measurement of Kolmogorov scale slender curved fibres

Vlad Giurgiu[1], Giuseppe C. A. Caridi[1], Mobin Alipour[2], Marco De Paoli[1,3], Alfredo Soldati[1,4]
1. TU Wien, Institute of Fluid Mechanics and Heat Transfer, Getreidemarkt 9, 1060, Vienna, Austria
2. Yale University, Department of Mechanical Engineering and Material Science, 17 Hillhouse Avenue, New Haven, Connecticut, U.S.A
3. University of Twente, Physics of Fluids Group, Drienerlolaan 5, 7522NB Enschede, The Netherlands
4. University of Udine, Polytehnic Department, 33100, Udine, Italy

Partikelverfolgung, Winkelgeschwindigkeit, Turbulenz, Kanalströmung
Particle tracking, angular velocity, turbulence, channel flow

Abstract

We measure the complete angular velocity of slender micro-plastic curved fibres in wall-bounded turbulence. The experiments are done in the TU Wien Turbulent Water Channel at shear Reynolds number 720. Fibre aspect ratio is 120 and their length is 8 Kolmogorov lengths. They are non-deformable, torsion-less, nearly neutrally buoyant, and have negligible inertia in these flow conditions. This study is original because previous experiments are limited to measuring rotation rates of large straight rods in homogeneous isotropic turbulence or restricted to tumbling rates only in turbulent channel flow. A 3D time-resolved particle image velocimetry system image the fibres in a close wall region. An established technique of fibre reconstruction and tracking is employed (Alipour et. al 2021) and extended. It consists of four steps: (i) the three-dimensional shape of each fibre is reconstructed with a tomographic algorithm, (ii) tracking, (iii) modelling of each fibre as a 2nd order polynomial, and (iv) determination of translation and rotation. The unique orientation over time is inferred and used to compute spinning and tumbling rates. We validate our in-house fibre code by generating synthetic fibres with known motion and perform a parameter sensitivity analysis. The uncertainty of the measured spinning rate is found to depend on the length of the minor axis of the curved fibre and its rotational rate. Finally, the ratio of mean spinning to tumbling rate was found higher than unity.

Introduction

The prediction of preferential orientation of anisotropic particles in turbulent flows is of importance because of the many implications it can have for industrial and environmental applications (Voth & Soldati 2017). Examples of relevant flows with anisotropic particles range from papermaking industry to environmental problems, such as sedimentation and micro-fibre pollution, among others. Natural fibres can have complex and non-regular shapes, difficult to systematically characterise. Therefore, many theoretical and numerical investigations have been focused on axisymmetric ellipsoids. The majority of experimental investigations consider rigid, isotropic particles with three planes of symmetry, e.g., rod- and disklike particles. In addition,

GALA e.V., Karlsruhe, Germany, ISBN 978-3-9816764-9-5

the imaging techniques adopted in previous works consist mainly in planar PIV measurements. In this study we use a three-dimensional and time-resolved imaging system to identify the orientation of the slender and curved fibers. The motion and rotation are computed with the technique presented by Alipour et al. (2021, 2022). The optical magnification is increased achieving higher 3D reconstruction resolution (50 voxel per fibre length) for a better determination of the fiber curvature, which in return, enables measurements of the spinning rate with lower uncertainty. As a result, the main parameters affecting the spinning rate uncertainty are discussed. Finally, tumbling and spinning rates of micro-fibres in a close-wall region of a turbulent channel flow are provided.

Facility and measurement setup

We perform fibre tracking measurements in the TU Wien Turbulent Water Channel (Fig. 1) at a shear Reynolds number of 720. This facility is a 10 m long transparent channel with an inner width-to-height aspect ratio of 10. The inner height is 80 mm. The channel is made of transparent polymethyl-methacrylate (PMMA) plates to allow optical access. The working fluid is water. A centrifugal volute pump circulates the water from the downstream to the upstream reservoir through four circular inlets. During experiments the water level is above the upper channel wall and the flow is driven through a converging inlet and into the channel by the pressure head generated in the upstream tank. After flowing through the measurement region water flows back to the downstream reservoir through a pipe and a regulation valve.

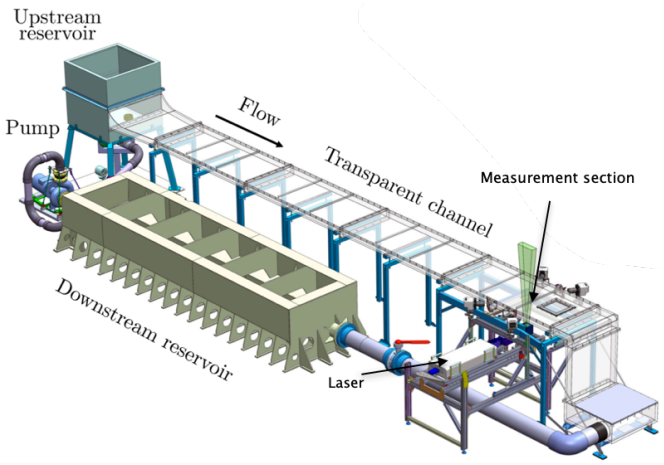

Fig. 1: Schematic of the TU Wien Turbulent Water Channel. Reproduced with permission from Alipour et al. (2021).

The facility is equipped with a control system which controls the shear Reynolds number within ± 0.1% (Giurgiu et. al 2023). The statistical properties of the produced flow are comparable to direct numerical simulations, being unaffected by the channel inlet or the side-walls (Giurgiu et. al 2023).
The measurement section is located 8.5 m downstream where a high-speed acquisition system is installed. The illumination is provided by a dual-cavity Nd:YAG Litron LD25-527 PIV laser and images are taken by six Phantom VEO 340L cameras at a frequency of 802Hz. They are equipped with Scheimpflug adapters and Tokina AT-X Pro 100mm macro lenses. The water is seeded with Polyamide spherical particles (density 1.15 kg/m^3 and diameter 20µm) and Polyamide fibres (density 1.15 kg/m^3) with length of 1.26 mm and diameter of 10µm.
Cameras are arranged in a cross-like configuration (Fig.2c) and they are focused on a volume of $40x34x15\ mm^3$ attached to the upper channel wall at the mid-span (Fig.2a,b). The initial

GALA e.V., Karlsruhe, Germany, ISBN 978-3-9816764-9-5

calibration is done with a LaVision 058-5 target. It achieved a fit error below 0.73px. The Volume self-calibration (Wieneke 2008) achieved an average disparity of 0.01voxel in 15x13x10 subdomains.

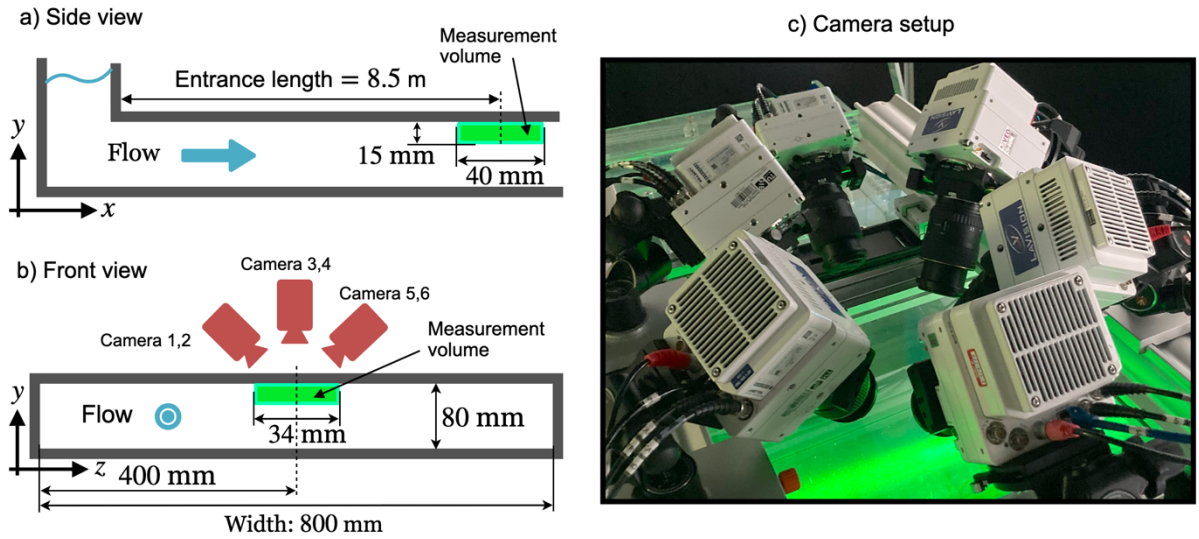

Fig. 2: Schematics (not to scale) and image of the measurement setup. The measurement location and size is shown in side view (a) and front view (b). The 6-camera cross-like setup is shown in panel c).

Tracking and rotation rates measurement method

We use an in-house tracking code to measure fibre rotation rates and we present the flowchart of the code in Fig.3. This procedure has been introduced by Alipour et al. (2021). We pre-processed the images by subtracting the minimum intensity over 10 frames and by using a spatial normalization of 300px. After image-processing of raw images and the calibration procedure presented in the previous section we perform a tomographic reconstruction of the illuminated measurement volume in DAVIS 10.2.1. We use the Multiplicative Algebraic Reconstruction Technique (MART) (Elsinga et al. 2006) in each time-step. The resulting objects which contain the reconstructed light intensity in each voxel are imported into MATLAB 9.13.0. Here we discriminate between tracers (used for calibration), reconstruction noise, and fibres based on the light intensity and size of connected regions. Then a threshold for the light intensity is chosen based on visual inspection of the objects. Any voxels with light intensities lower than this threshold are disregarded. Secondly, connected regions of voxel are identified. Regions having one size in voxels bigger than a threshold are kept. This threshold is determined by considering the nominal length of the used fibres and optical magnification. Spherical objects (tracers and noise) are smaller than elongated connected regions and this allows for a well-defined differentiation. Thus, the remaining regions are identified as fibres. The temporal evolution of their center of mass is used for tracking. This is based on a simple search-radius procedure. This approach is possible, because we study dilute concentrations, e.g. 30 fibres each 50 voxels long and 6 voxels in diameter in our measurement volume represent a volumetric concentration of 10^{-4} fibre voxels/ measurement volume voxels.

GALA e.V., Karlsruhe, Germany, ISBN 978-3-9816764-9-5

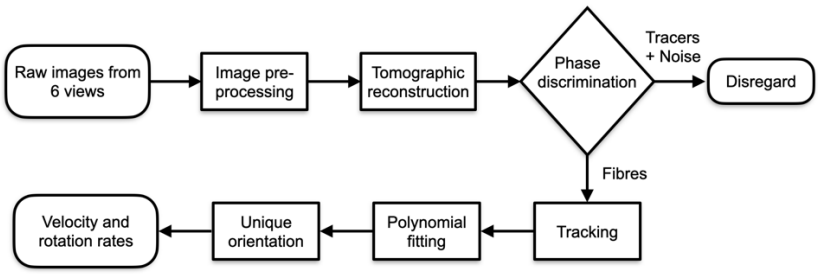

Fig. 3: Flow-chart of the method used to measure translational and rotational velocities of fibres.

The fibres are contained within a plane and are rigid (Alipour et al. 2021). They are curved and this allows fitting a 2nd order polynomial through each fiber. The x,y, and z positions of each voxel of a fibre are fitted through a linear least-squares procedure to a curvilinear coordinate s which connects all voxels within a fibre. This results in 3 polynomials x(s), y(s), and z(s) which correspond to the three-dimensional coordinates of the searched polynomial approximating the fibre object. An example of this fitting procedure is shown in Fig. 4. The unique fibre reference frame $(\vec{x'}, \vec{y'}, \vec{z'})$ is found by computing the eigenvectors of the moment of inertia tensor of the fitted polynomial (black line in Fig.4) with respect to its centre of mass. The eigenvectors $\vec{x'}$, $\vec{y'}$, and $\vec{z'}$ correspond to the lowest, intermediate, and highest eigenvalues, respectively.
We define the rotation matrix of the fibre reference frame with respect to the laboratory reference frame (the identity matrix) in each time-step as $\mathbf{R}$. In the first, second, and third column of this matrix the components of the $\vec{x'}$, $\vec{y'}$, and $\vec{z'}$ vectors are placed. We use the temporal evolution of $\mathbf{R}$ to compute fibre rotation rates with respect to the fibre reference frame through two methods. Rotation around the axis defined by $\vec{x'}$ is called spinning ($\omega_{x'}$) and combined rotation around $\vec{y'}$ and $\vec{z'}$ is called tumbling ($(\omega_{y'}{}^2 + \omega_{z'}{}^2)^{1/2}$) (Soldati and Voth 2017).

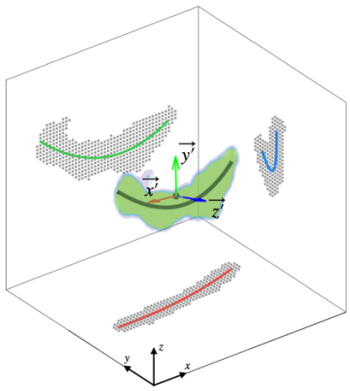

Fig. 4: Projections (grey dots) of the fibre onto the planes xy, xz, zy are fitted by 2nd order polynomials (red, green, and blue) which are used to generate the fibre-fitted polynomial (black line). The laboratory reference frame is shown as black arrows. The fibre reference frame is shown as red, green, and blue arrows. The bounding box is 60^3 voxels.

First, we use an algebraic method to compute the fibre rotation rates from the rotation matrix, $\mathbf{R}$, and its time derivative, $\dot{\mathbf{R}}$ (Coutinho 2012):

$$\boldsymbol{\Omega}_f = \mathbf{R}^{-1}\dot{\mathbf{R}}\,,$$

where $\boldsymbol{\Omega}_f$ is a skew-symmetric matrix and contains the rotations rates (spinning and tumbling) around the fibre reference frame (subscript f):

GALA e.V., Karlsruhe, Germany, ISBN 978-3-9816764-9-5

$$\mathbf{\Omega}_f = \begin{pmatrix} 0 & \omega_{z'} & \omega_{y'} \\ \omega_{z'} & 0 & -\omega_{x'} \\ -\omega_{y'} & \omega_{x'} & 0 \end{pmatrix}.$$

Secondly, we use a method based on quaternion calculus as Zhao and Van Wachem (2013), Lecrivain et al. (2020), among others. In contrast to Alipour et al. (2021), we don't use Euler angles to represent orientations to avoid the Euler angle singularity. It is defined as the non-uniqueness of Euler angles when attempting to represent particular orientations (Greenwood 1988). Instead, we directly use the rotation matrix $\mathbf{R}$ to compute the quaternion representing the orientation for each time-step (Coutinho 2012). We compute the temporal change of the components of the quaternion and finally we compute the angular velocity vector (Coutinho 2012), which we project on the fibre orientation vectors to obtain the spinning and tumbling rates.

Code verification and uncertainty quantification

To verify our in-house tracking code, we generate synthetic fibres to which we apply known translations and angular velocities. This is achieved in three steps: i) a 2nd order polynomial representing a curved fibre is generated, ii) the fiber is translated and rotated, and iii) a volume in voxel is generated around the polynomial similar to the MART reconstructed objects. This object is used in our tracking code and we show one synthetic fibre (length of 80 voxel) trajectory in Fig. 5a. The fibre geometry is defined by the major axis L' (70 voxel) and minor axis l' (17 voxel). Fig. 5.b,c show the comparison between the input rotation rate (green lines) and the output of the tracking code (red and blue dots). We observe good agreement between the two used methods (algebraic and quaternion). In this example, the standard deviation of the measured spinning rate is $0.052°/s$, while the one for tumbling is 3 times lower.

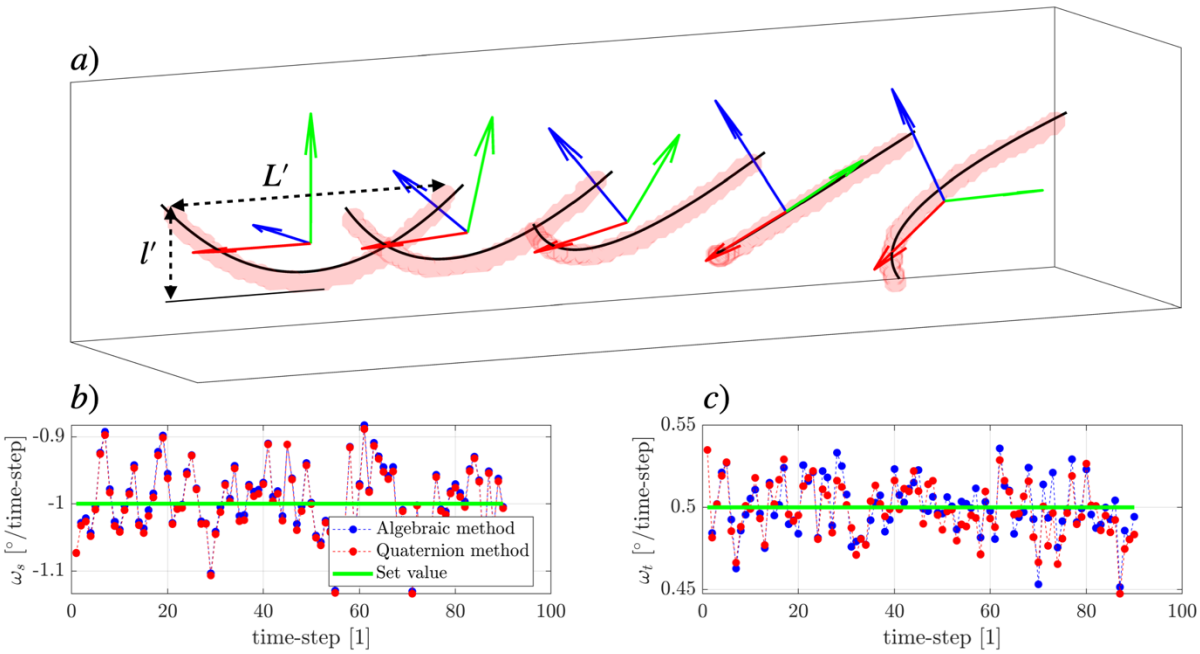

Fig. 5: A synthetic fibre at different time-steps is shown in panel a). Panel b) and c) show the measured spinning and tumbling rate, respectively. The fibre was generated with the rotation rates indicated by the set values (green lines).

GALA e.V., Karlsruhe, Germany, ISBN 978-3-9816764-9-5

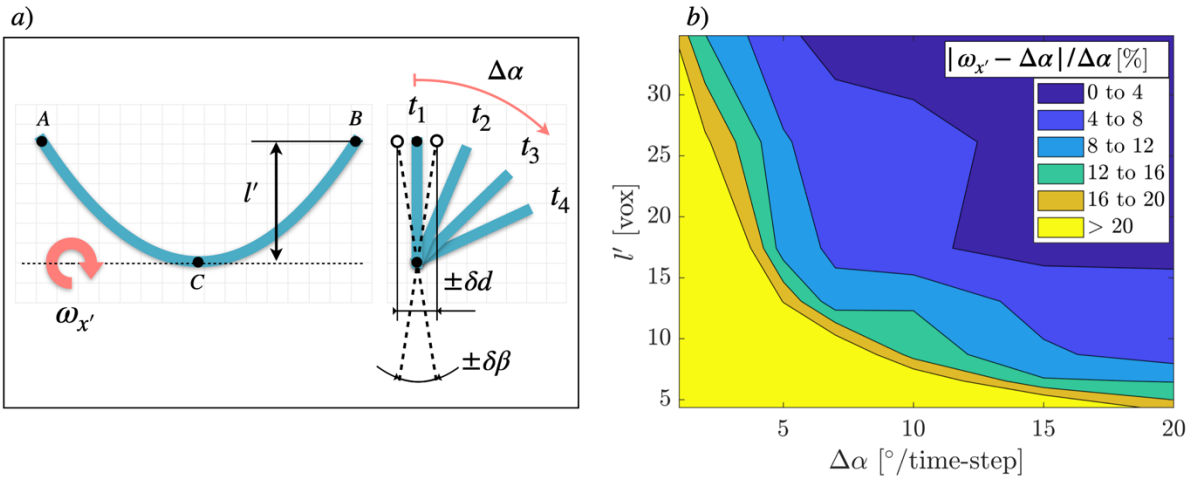

Fig. 6: Schematic of spinning rate uncertainty is shown in panel a). Spinning rate error map as function of minor axis length (l') and angular displacement ($\Delta\alpha$) is shown in panel b).

The main parameters affecting the uncertainty of the spinning rate of a curved fiber are the minor axis l' and the rotational rate, $\Delta\alpha$ as illustrated in Fig.6a. Here the fiber is represented by only 3 points A, B, C which define the fibre-containing plane. Due to discretization errors – fibre represented by voxels – the relative position of points A and B with respect to C has the uncertainty δd in front view (Fig.8.a right). The fibre-containing plane (i.e., the orientation around the spinning axis) has thus an uncertainty in inclination of $\delta\beta = arctan(\delta d/l')$, where l' is the length of the minor axis. The uncertainty of the spinning rate depends on the ratio between the angular displacement per time-step ($\Delta\alpha$) of the fibre-containing plane between two time-steps and its uncertainty in inclination. To quantify the error of spinning rate we generate synthetic fibres with the same shape, but different resolutions, i.e., different minor axis lengths in voxels, and different angular displacements per time-step and use our fibre tracking code to measure the spinning rate ($\omega_{x'}$). In Fig.6.b. we provide an error map of the spinning rate as function of l' and $\Delta\alpha$. We observe that with increasing l' the error decreases, because the uncertainty in inclination of the fibre-containing plane decreases. Moreover, we observe that with increasing $\Delta\alpha$ the error decreases, because the angular displacement becomes increasingly larger than the inclination uncertainty of the fibre plane.

Measured rotation rates

We reconstruct the trajectory of one fibre and show it in Fig.7.a. It has a minor axis length of $\sim 10\ vox$. For the computation of the rotation rates, we consider the rotation matrix of every 10^{th} time-step achieving a spinning angular displacement of $\sim 20°$ between the two time-steps considered. Using the map of Fig.6b. we estimate the uncertainty of the spinning rate below 8%. Based on the observation of the measured rotation rates of the synthetic fibre in Fig. 5. we infer that uncertainties on the tumbling rate are similar or lower than those on the spinning rate. Moreover, we apply a Savitzky-Golay of 2^{nd} order with a kernel of 40 time-steps to the components of the orientation vectors of this fibre. The kernel size has been chosen based on observing the temporal evolution of these vectorial components (not shown here). We show the measured spinning and tumbling rates of this fibre in Fig.7.b and Fig.7.c, respectively. We observe that both methods used for the rotation rates computation are in good agreement. Moreover, we observe higher mean spinning than tumbling rate.

GALA e.V., Karlsruhe, Germany, ISBN 978-3-9816764-9-5

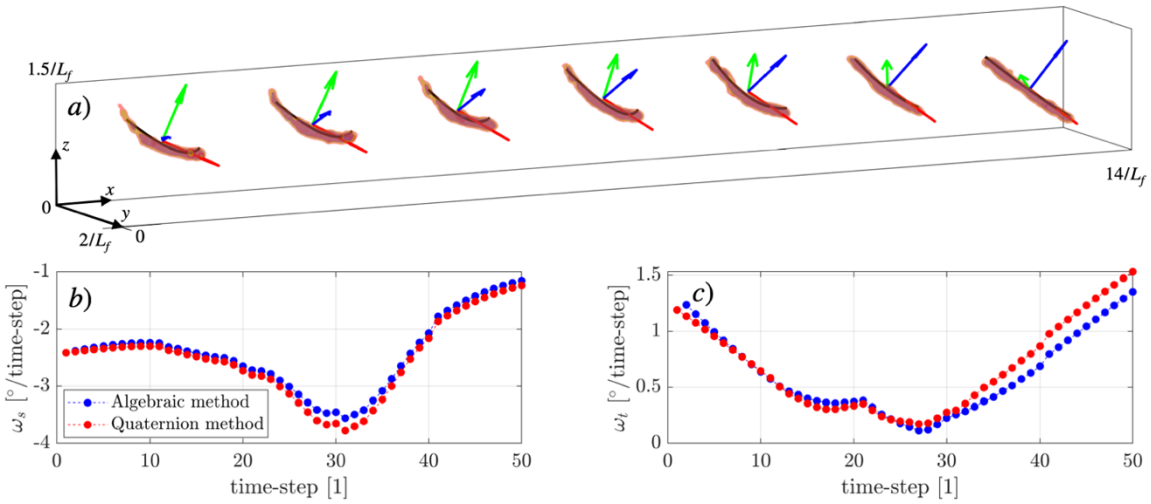

Fig. 7: Example fibre track and measured rotation rates. Panel a) shows the reconstructed fibre at 7 time-steps. The trajectory is shown up to time-step 35 and only every 5th fibre is shown. Fitted 2nd order polynomial (black line) and orientation vectors (red, green, and blue vectors) are shown. Panel b) and c) show the spinning and tumbling rates, respectively.

We tracked ~ 1000 fibres in the region close to the wall below 280 viscous lengths to investigate if on average spinning rates are higher than tumbling rates. Moreover, we investigated the effect of the fibre shape on the mean rotation rates. To achieve this comparison, we use the definition of Alipour et al. (2021) of the dimensionless curvature $\kappa* = \kappa/\kappa_0$, where κ is the mean curvature of the fibre and $\kappa_0 = \pi/\overline{L_f} = 2.53\, mm^{-1}$ is the curvature of an arc having the nominal length of the used fibres $\overline{L_f} = 1.26\, mm$ and the shape of half a circle. The three curvature classes are 1) $0 < \kappa* < 0.28$, 2) $0.28 < \kappa* < 0.42$, and 3) $0.42 < \kappa*$ (Alipour et al. 2021). In Fig.8 we show spinning and tumbling rates times the Kolmogorov timescale ($\tau_\eta \sim 25ms$ – estimated based on DNS (Moser et al. 1999) at shear Reynolds number 590) for the three dimensionless curvature classes. We observe rotation rates slower than the turn-over time of Kolmogorov-sized eddies. This is motivated by the fact that the used fibres are 8 Kolmogorov length scales long and thus the action of multiple eddies integrate over the fibre length. We don't observe a dependence of the spinning and tumbling rates on the curvature. The spinning rate for the lowest curvature class has the highest uncertainty (lower curvature fibres have a smaller minor axis length – see Fig.6.b) and thus cannot be considered different from the spinning rate of the other two curvature classes. The mean spinning rates were found higher than the tumbling rates for all curvatures.

Conclusion

In this work, we present the methodology used to measure spinning and tumbling rates of curved fibres (length of $1.26\, mm$) in turbulence. The experiment is performed in the TU Wien Turbulent Water channel at a shear Reynolds number of 720 in a close-wall region extending up to 280 viscous lengths. We verify our tracking code by generating synthetic fibres with set spinning and tumbling rates and we provide an uncertainty quantification for the spinning rates. Finally, we measure the mean spinning and tumbling rates of ~ 1000 fibres and find that they spin faster than they tumble, but spin and tumble slower than Kolmogorov sized eddies. We don't find a dependence of the rotation rates on their curvature.

GALA e.V., Karlsruhe, Germany, ISBN 978-3-9816764-9-5

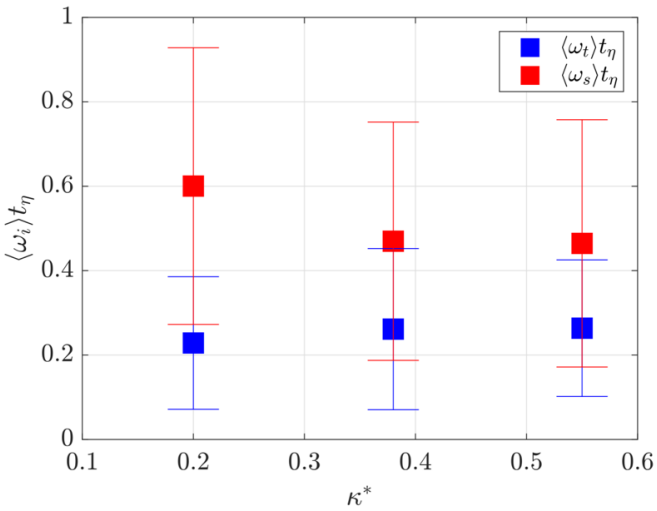

Fig. 8: Mean tumbling ($\omega_t = (\omega_{y'}^2 + \omega_{z'}^2)^{1/2}$) and spinning rates ($\omega_s = \omega_{x'}$) times the Kolmogorov time-scale over dimensionless curvature are shown. The error bars represent ± 1 standard deviation.

Acknowledgments

The authors acknowledge the TU Wien University Library for financial support through its Open Access Funding Program. This research was funded in part by the Austrian Science Fund (FWF) [Grant No. J-4612]. V.G. acknowledges the financial support provided by FSE S3 HEaD (grant no. 1619942002) and CLEANSTONE Interreg V-A Italia-Austria (grant no. ITAT1419-P). This research was funded in part by the Austrian Science Fund (FWF) [Grant No. P-35505]. V.G. and A.S. also gratefully acknowledge funding from the PRIN project "Advanced computations and experiments in turbulent multiphase flow" (project no. 2017RSH3JY).

Literatur

Alipour, M., De Paoli, M., Ghaemi, S., & Soldati, A. 2021. "Long non-axisymmetric fibres in turbulent channel flow". Journal of Fluid Mechanics, 916, A3.
Coutinho, M.G. 2012: "Guide to dynamic simulations of rigid bodies and particle systems", Springer Science & Business Media.
Elsinga, G. E., Scarano, F., Wieneke, B, & Oudheusden, B. W. 2006. "Tomographic particle image velocimetry". Experiments in Fluids, 41, 933-947.
Giurgiu, V., Caridi C. A. G., Alipour, M., De Paoli, M., & Soldati, A. 2023. "The TU Wien Turbulent Water Channel: flow control loop and three-dimensional reconstruction of anisotropic particle dynamics". Review of Scientific Instruments. (in review)
Greenwood, D.T. 1988: "Principles of dynamics", NJ: Prentice-Hall, Vol. 21, No. 6.
Lecrivain, G., Grein, T. B. P., Yamamoto, R., Hampel, U., & Taniguchi, T. 2020. "Eulerian/Lagrangian formulation for the elasto-capillary deformation of a flexible fibre". Journal of Computational Physics, 409, 109324.
Moser, R. D., Kim, J., Mansour, N. N. 1999. "Direct numerical simulation of turbulent channel flow up to $Re_\tau = 590$". Experiments in Fluids, 41, 933-947.
Voth, G. A., Soldati, A., 2017. "Anisotropic particles in turbulence". Annual Review of Fluid Mechanics, 49, 249-276.
Wieneke, B. 2008. "Volume self-calibration for 3D particle image velocimetry". Experiments in Fluids, 45, no.4, 549-556.
Zhao, F., & Van Wachem, B. G. M. 2013. "A novel Quaternion integration approach for describing the behaviour of non-spherical particles". Acta Mechanica, 224(12), 3091-3109.

GALA e.V., Karlsruhe, Germany, ISBN 978-3-9816764-9-5